Spring 5-1-2015

Electrostatic Assembly of Gold Nanoparticles Mediated by Polyoxomolybdates

Shannon M. Walter
Syracuse University

Abstract

The electrostatic assembly of cationic gold nanoparticles (AuNPs) with core diameters of approximately 1.5 nm and 4.5 nm and the anionic sphere and wheel polyoxomolybdates $(NH_4)_{42}\left[Mo^{VI}_{72}Mo^{V}_{60}O_{372}(CH_3COO)_{30}(H_2O)_{72}\right]\cdot$ ca. 300 $H_2O\cdot$ ca. 10 CH_3COONH_4 (Mo-132a), $(NH_4)_{72\text{-}n}\left[\left\{(H_2O)_{81\text{-}n}+(NH_4)_n\right\}\subset\left\{\left(Mo^{VI}\right)Mo^{VI}_5O_{21}(H_2O)_6\right\}_{12}\left\{Mo^{V}_2O_4(SO_4)\right\}_{30}\right]\cdot$ ca. 200 H_2O (Mo-132b), and $(NH_4)_{28}\left[Mo_{154}(NO)_{14}O_{448}H_{14}(H_2O)_{70}\right]\cdot 350\ H_2O$ (Mo-154) was investigated. The AuNPs were capped with a trimethylammonium terminated ligand. Zeta potential and UV-Vis studies supported the successful assembly of the oppositely charged species. The ratio at which the precipitation of aggregates from solution occurred was consistent with the point of electroneutrality observed in the zeta potential results. The UV-Vis studies showed the loss of the surface plasmon resonance (SPR) band as this point of electroneutrality was approached.

In a study performed by Gooch, *et. al.* involving combining the 4.5 nm AuNP and Mo-132a and Mo-132b, it was found that a counterintuitive trend was observed. The precipitation point for the more negatively charged Mo-132b corresponded to a higher ratio than the precipitation point for Mo-132a. This trend continued in this study involving the 4.5 nm AuNP and Mo-154, where r = [POM]:[AuNP] mole ratio of $r \approx 8$ was required to reach the point of electroneutrality and precipitation than what would be predicted through basic charge balance considerations. In the study involving the 1.5 nm AuNP, the spherical Mo-132 Keplerates precipitated out approximately at the point where the charges on the nanoparticles and polyoxomolybdates were balanced, similar to what is observed when oppositely charged nanoparticles interact. These ratios for Mo-132a and Mo-132b were $r \approx 1$ and $r \approx 0.6$, respectively. However, the precipitation point between the smaller AuNP and Mo-154 again required less of the Mo-154 than what would be expected if it followed this trend at $r \approx 0.4$. Overall, these results indicate that both the shape and charge of the polyoxomolybdate and the size of the AuNP affect their interaction and precipitation point.

Executive Summary

In the present work, the electrostatic assembly of polyoxomolybdates and gold nanoparticles was investigated. Polyoxometalates (POMs) are frameworks comprised of multiple metal ions bridged by oxygens. They can contain different kinds of metals and are also capable of incorporating heteroatoms, such as phosphorous, sulfur, or nitrogen. A central metal ion forms a polyhedron with the atoms bonded to it, and several polyhedra come together to form the polyoxometalate. Due to the diversity of coordination polyhedra that can be formed and the variety of ways they can connect, a vast assortment of overall shapes and structures are possible. They can even be built to a size beyond the molecular scale of 0.1-10 nm (1 nm = 10^{-9} m) and into the nanoscale of 1-100 nm. This assortment of structures is what makes POMs a subject of interest in current research. They can be synthesized to display a variety of desirable properties, such as luminescence or mesoporosity where any cavities or channels are well-defined. Typically, polyoxometalates are anions, meaning they have an overall negative charge.

Polyoxomolybdates or POMs are clusters where the only metal present in the structure is molybdenum. In the present work, three polyoxomolybdates were used, two of which were spherical (Mo-132), and one which was shaped like a wheel (Mo-154).

Similarly, nanoparticles are materials whose size lies between 1-100 nm, and are interesting due to the fact that they exhibit properties that are not observed at either the molecular or bulk scales. Metal nanoparticles are typically comprised of a neutral metal core with ligands adsorbed onto the surface. With regards to nanoparticles, ligands are generally long chain organic molecules that can bind to the surface of the metal core. For gold nanoparticles (AuNPs), there is normally a thiol group at one end of the chain, containing a sulfur-hydrogen group. There is a strong affinity between sulfur and gold, making the bond between them strong and keeping

the ligands attached. The other end of the chain can be terminated with a charged functional group to give the nanoparticles an overall charge, either positive or negative. In the present work, the nanoparticles used contained a spherical gold core of varying sizes surrounded by positively charged ligands.

Most current research involving nano-sized units is focused on building larger systems from these nano-objects rather than developing new nanoparticles, such as systems involving POMs and AuNPs. This is partially due to the fact that many of the possible applications for nanoparticles rely on how these nanoscopic entities come together and interact, rather than the effects of a single nano-object. Because of this, understanding how nano-sized objects aggregate is important in the design of nanomaterials. The potential applications for these nanomaterials include electronics, drug delivery, and catalysis, where the nanomaterial can speed up the rate at which a reaction proceeds and is not consumed.

With regards to nanoparticles, it has been found that a mixture containing two types of nanoparticles, one positively charged and the other negatively charged, will precipitate from solution only when the overall charge between the two types are balanced. This has led to the electrostatic assembly of charged nanoparticles, where the attraction between the positively charged ligands on one nanoparticle and the negatively charged ligands on another nanoparticle led to aggregation and assembly of nanoscopic entities. This electrostatic assembly has even led to the development of crystals constructed from two types of oppositely charged nanoparticles. However, in a recently published study involving AuNPs and POMs, a trend counterintuitive to this was observed. That study involved combining one type of AuNP with POMs of differing negative charges. It was found that a larger amount of the more negatively charged POM was required for precipitation to occur than the amount required in the system with the less

negatively charged POM. Had those systems followed the trend observed with oppositely charged nanoparticles, a smaller amount of the more negatively charged POM would have been needed. This observation was mainly explained by the different ways that the counterions that balanced out the charges of the POMs interact with the counterions of the AuNPs and with the POM itself.

The aim of this project was to further investigate this concept of the precipitation point dependence on charge neutrality between oppositely charged nano-sized species. This was done by combining positively charged nanoparticles and negatively charged polyoxomolybdates and observing how they interact by finding the ratio at which precipitation occurs. Two nanoparticles were used, both with the same positively charged ligand but with different diameters of the metal core. The different sizes of the core meant that these nanoparticles had different overall charges, where a larger core was covered with more ligands and therefore had a higher charge. Three polyoxomolybdates were used as well, two of which were spherical and one was shaped like a wheel. All three had differing overall negative charges.

The general experimental procedure employed separate vials containing one size of nanoparticle. A solution of one of the types of polyoxomolybdates was added to the vials in different amounts, providing a range of ratios between the positively charged nanoparticles and the negatively charged polyoxomolybdates. The ratio at which aggregation and precipitation occurred was observed, then the systems were analyzed using zeta potential and ultraviolet-visible spectroscopy. In all of the studies, the zeta potential results supported what was observed visually where the point of electroneutrality occurred at the same ratio where precipitation occurred. Zeta potential essentially provides a way of measuring the stability of suspended charged particles, where precipitation generally occurs when the measured potential is near zero.

This indicates that the electrostatic repulsive forces between like-charged entities is not strong enough to keep the particles suspended, and therefore aggregation and precipitation occur. In ultraviolet-visible spectroscopy, the wavelengths at which absorption occurs can be characteristic of the entities present in solution.

Based on the previous study involving oppositely charged AuNPs and POMs, it was expected that the systems investigated here would behave similarly and precipitate out in a manner counterintuitive to the studies involving oppositely charged NPs. However, this result was only observed with the same-sized nanoparticle as that which was used in the previous study. In the studies performed with a smaller nanoparticle, it was found that the spherical Mo-132 entities precipitated out according to the approximate point of charge balance between the AuNPs and POMs, similar to what is observed when oppositely charged nanoparticles are combined. However, the precipitation point between the smaller AuNP and the Mo-154 occurred at a lower ratio than what would be expected if it were to follow the trend observed with the other POMs and the same-sized NP. Overall, these results indicate that both the shape and charge of the POM and the size of the AuNP affect their interaction and precipitation point.

Table of Contents

Abstract ..... **i**
Executive Summary ..... **ii**

1 Introduction **1**
1.1 Nanoparticles 1
1.2 Zeta Potential 2
1.3 Precipitation Across Size Regimes 3
1.4 Polyoxomolybdates 5
1.4.1 Mo-132: Keplerates 6
1.4.2 Mo-154: the “Big Wheel” 8
1.5 Literature Review 10

2 Experimental Methods **12**
2.1 Synthesis of Polyoxomolybdates 12
2.1.1 Synthesis of Mo-132a 12
2.1.2 Synthesis of Mo-132b 13
2.1.3 Synthesis of Mo-154 13
2.2 Synthesis of Gold Nanoparticles 13
2.2.1 Synthesis of $Au_{1.5}$TMA ($Au_{1.5}$) 13
2.2.2 Synthesis of $Au_{4.5}$TMA ($Au_{4.5}$) 15
2.3 Sample Preparation and Analysis 16
2.4 Instrumentation 16
2.4.1 Zeta Potential and Dynamic Light Scattering (DLS) 16
2.4.2 Ultraviolet-Visible Spectroscopy (UV-Vis) 16
2.4.3 Thermogravimetric Analysis (TGA) 17
2.4.4 Transmission Electron Microscopy (TEM) 17

3 Results and Discussion **17**
3.1 Keplerates and AuTMA Studies 17
3.1.1 Mo-132a and $Au_{1.5}$TMA 17
3.1.2 Mo-132b and $Au_{1.5}$TMA 19
3.2 Mo-154 and AuTMA Studies 22
3.2.1 Mo-154 and $Au_{1.5}$TMA 22
3.2.2 Mo-154 and $Au_{4.5}$TMA 26

4 Conclusions and Future Work **28**

5 References **31**

Appendix A Abbreviations **35**
Appendix B Thermogravimetric Analysis **37**

1 Introduction

1.1 Nanoparticles

Nanoparticles (NPs) are of interest due to the variety of applications, quantum size effects, and the behavior of individual NPs. They exhibit physical properties that are not displayed by either the bulk metal or molecular compounds due to quantum-mechanical rules related to their electronic structure.[1,2] These properties depend on size, distance between NPs, type of ligand, and shape.[1,3] Their potential applications include catalysis, electronics, energy storage, and biological applications such as drug delivery.[1,2,4-8]

Interest in gold nanoparticles (AuNPs) generally comes from the fact that they are the most stable metal nanoparticle.[1] A basic description of their synthesis involves adding a reducing agent to a gold salt as well as a charged stabilizing agent or surfactant to provide colloidal stability to the NPs by keeping them separated through electrostatic repulsion. Gold nanoparticles can forma a variety of shapes, such as spheres, rods, or hollow shells. The stabilizing agent/surfactant can be replaced through ligand exchange, which for AuNPs is typically a thiol due to the high affinity between sulfur and gold.[1,3,5] It is advantageous to use ligands which will form a self-assembled monolayer (SAM), where the ligands organize on their own in a compact manner on the surface of the core. This makes it energetically unfavorable to disrupt the SAM, making the nanoparticle more stable.[3] Charges can easily be added to the NPs by using ligands terminated by a charged functional group[8], such as positively charged N,N,N-trimethyl(11-mercaptoundecyl)ammonium chloride (TMA).

Nanoparticles can be characterized through such methods as ultraviolet-visible spectroscopy (UV-Vis), electron microscopy, dynamic light scattering (DLS), and electrophoresis. The absorption band observed in UV-Vis spectra for nanoparticles is known as

the surface plasmon resonance (SPR) band. It arises when the free electrons are excited as a group and oscillate upon absorption.[3,5] The resonance arises when the frequency of the incident light and the frequency of the electron cloud oscillation are the same (Fig. 1). This oscillation of the electrons is called the surface plasmon, and absorption occurs very strongly near this frequency. Noble metal NPs tend to have strong plasmon resonances in the visible light range, giving them a vivid color in solution. This SPR band depends on the size of the metal core; as the size increases, the SPR band undergoes a red-shift to higher wavelengths. This red shift causes the suspension to appear more violet or blue, and can also occur when the particles aggregate. For AuNPs, the SPR band is usually centered around 510-530 nm for gold core diameters of around 4-40 nm.[3,5]

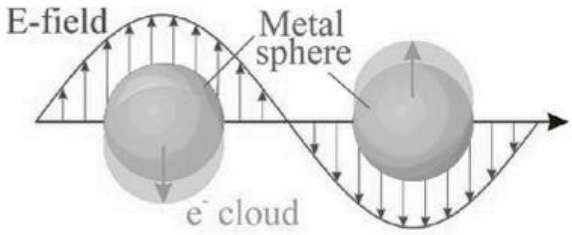

Fig. 1: Diagram showing how surface plasmon resonance arises in spherical metal nanoparticles. When the frequency of the incident light (E-field) and the frequency of the oscillation of the electron cloud (e- cloud) are the same, it leads to the surface plasmon resonance.[3]

1.2 Zeta Potential

A charged particle in solution will attract ions of opposite charge which will be strongly bound to the surface of the particle. This layer is known as the Stern layer and shields the surface charge of the particle.[9,10] Beyond this layer of ions is the diffuse layer, which is more loosely bound to the particle. These layers make up the electric double layer where the outer boundary is known as the slipping plane. When an electric field is applied to the solution, the slipping plane is the boundary of ions which move with the charged particle, while ions outside the slipping

plane remain unaffected by the movement of the particle. The zeta potential is the potential at this plane (Fig. 2).[11,12]

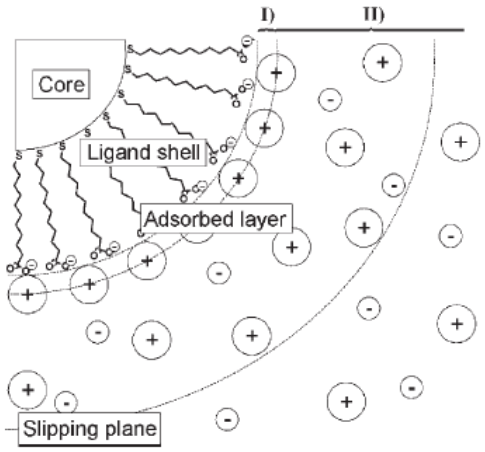

Fig. 2: Graphic representation of the electric double layer for a nanoparticle functionalized with a negatively charged ligand. Labeled are the metal core of the NP ("Core"), the bound ligands ("Ligand shell"), the Stern layer of adsorbed countercations ("Adsorbed layer"), and the plane of shear ("Slipping plane"). The zeta potential is the potential at the slipping plane.[11]

Zeta potential is not a direct measure of the charge of a particle, but rather it is related to the charge which leads to electrostatic repulsions between like-charged particles. Zeta potential values of large magnitude are more stable than smaller values. The smaller values indicate that particles will have a tendency to flocculate, or aggregate, as the colloidal system is not as stable due to a weaker electrostatic repulsive force.[9] This repulsive force is very important in maintaining the stability of a colloidal suspension (e.g. nanoparticle dispersion system), as it is only when the repulsive forces are greater than the attractive van der Waals interactions that the particles remained dispersed.[13]

1.3 Precipitation Across Size Regimes

The level of stability of mixtures of oppositely charged species in solution depends on their size (Fig. 3). Larger particles in the micro size regime precipitate out continuously due to a combination of residual van der Waals forces leading to attraction between microparticles and

the weak solvation of large aggregates. On the molecular level, complexing ions will precipitate out when they reach a certain ratio due to solubility and equilibrium. In contrast, oppositely charged nanoparticles will precipitate out once they reach the point of electroneutrality and a neutral surface charge on the resulting aggregates.[14]

When oppositely charged nanoparticles are combined below the point of charge compensation, they will initially form small aggregates that are stabilized by a shell of the dominant charged species. This stabilizes the aggregates through solvation and electrostatic repulsion between the like-charged shells, preventing further aggregation. As the point of electroneutrality is approached, the aggregates become larger and larger where the outer shell of the more concentrated nanoparticle surrounds both the positively and negatively charged NPs. At the point of electroneutrality, there aren't enough of the more concentrated nanoparticle to form the stabilizing shells the stabilizing effects no longer apply, leading to precipitation.[14,15] It would be expected for the like-charged repulsive force between the "shell" NPs to be too large for the shell to form. However, the ions in solution screen the charges of the nanoparticles, allowing the shells to form.[8]

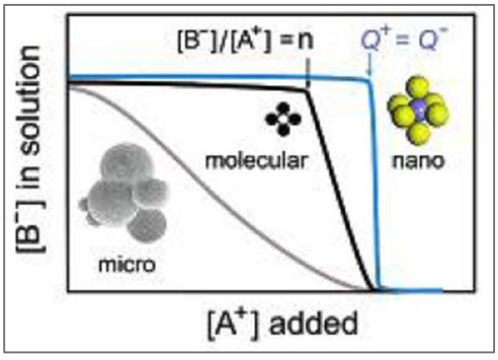

Fig. 3: Graph describing how the precipitation of oppositely charged particles depends on their size. Microparticles precipitate out continuously, complexing ions on the molecular level precipitate out when a certain ratio between the ions has been reached, and nanoparticles precipitate out when the oppositely charged particles reach electroneutrality.[14]

1.4 Polyoxomolybdates

In general, polyoxometalates (POMs) can form a wide variety of structures.[16,17] However, scientists have had issues with synthesizing compounds and materials with desirable properties, such as mesoporosity (where the cluster has well-defined openings), luminescence, and catalytic activity.[16,18-21] POMs are specifically of interest here due to their ability to form structures whose sizes lie in the mesoscopic size regime, which lies between the microscopic world of small molecules and the macroscopic world of 'bulk' compounds.[16,17] This puts them in the same sized order of magnitude as nanoparticles. The structures of POMs are based on the linking of metal-oxide polyhedra, allowing for the diverse assortment of structures which include spheres and wheels.[16] These large clusters can even themselves be used as building blocks, where the spheres or wheels can be linked together in chains or layers.[17-27]

Polyoxomolybdates are especially good at being able to create various shapes and structures for various reasons. Some of these are: the simple way of changing coordination numbers, the easy ways of performing ligand exchange between water and other ligands at molybdenum sites, the ability to adjust or increase the electron density without forming metal-metal bonds, and terminal Mo=O groups hindering linking and preventing unrestrained growth.[28] Many polyoxomolybdates can be synthesized using the basic process of acidifying an aqueous molybdate solution and then adding a reducing agent. The final product depends on the length of time the reaction is allowed to proceed, the pH, the ionic strength of the solution, the type of electrolytes present, the concentration of molybdate, the concentration of the reducing agent, and the type of reducing agent.[23,29] Reduction of anions, either a single polyhedron or a building block, leads to a higher charge density on the peripheral oxygens due to the increased magnitude of the overall negative charge. This leads to protonation, which could lead to additional

condensation reactions to expand the fragment. It is through this type of growth that many polyoxomolybdates are constructed.[29]

1.4.1 Mo-132: Keplerates

When Keplerates (Mo-132) were first discovered, they were considered quite remarkable due to their high symmetry and spherical shape as icosahedral inorganic superfullerenes.[22] Each Mo-132 is made up of 12 $\{Mo_{11}\}$ moieties, giving each 132 molybdenum atoms. Each $\{Mo_{11}\}$ unit has a C_5 symmetry and contains a central $\{MoO_7\}$ pentagonal bipyramid surrounded by 10 $\{MoO_6\}$ octahedra (Fig. 4).[22,29-33]

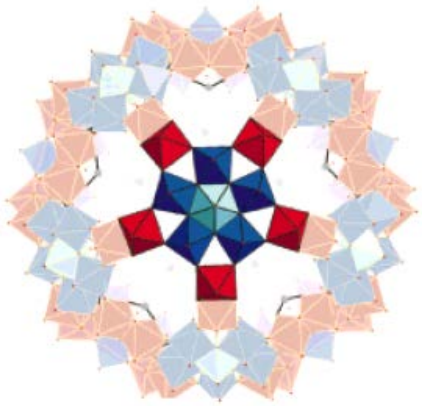

Fig. 4: Polyhedral representation of a Keplerate (Mo-132). Shown in darker colors is the $\{Mo_{11}\}$ unit with C_5 symmetry. In the center is the $\{MoO_7\}$ pentagonal bipyramid, which is surrounded by 10 $\{MoO_6\}$ octahedra. Mo-132 spheres contain 12 of these units.[34]

These spheres can also be thought of as consisting of 12 $\{(Mo)Mo_5\}$ pentagons linked together by 30 $\{Mo_2^{V}O_4\}^{2+}$, and the $\{Mo_2^{V}O_4\}^{2+}$ are bridged with a bidentate ligand (Fig. 5). This classical $\{Mo_2^{V}O_4\}^{2+}$ linker is usually formed in solutions of reduced molybdates and bidentate ligands. When an Mo-132 type Keplerate is made using acetate, Mo-132a is formed:

$$(NH_4)_{42}\left[Mo_{72}^{VI}Mo_{60}^{V}O_{372}(CH_3COO)_{30}(H_2O)_{72}\right]\cdot \text{ ca. } 300\ H_2O \cdot \text{ ca. } 10\ CH_3COONH_4$$

(Mo-132a).[22,30] If the bidentate ligand used is sulfate instead of acetate, Mo-132b is formed:

$$(NH_4)_{72-n}\left[\left\{(H_2O)_{81-n}+(NH_4)_n\right\}\subset\left\{\left(Mo^{VI}\right)Mo_5^{VI}O_{21}(H_2O)_6\right\}_{12}\left\{Mo_2^{V}O_4(SO_4)\right\}_{30}\right]\cdot \text{ca. } 200\ H_2O$$

(Mo-132b).[35,36]

The actual cage forming the sphere has an overall charge of -12, with 30 binding sites for ligands. Since acetate is a monovalent ligand with a -1 charge and sulfate is a divalent ligand with a -2 charge, this difference in ligand leads to Mo-132a having an overall -42 charge while Mo-132b has an overall -72 charge.[30,33,35,36] This increased negative charge on Mo-132b leads to an increased affinity for the countercations and their encapsulation. Both Mo-132a and Mo-132b could encapsulate their NH_4 counterions, which would affect their overall charges, however this was not considered.[35]

Fig. 5: Polyhedral representation of the {(Mo)Mo_5} unit present in Mo-132. In the center (light blue) is a {MoO_7} pentagonal bipyramid, surrounded by five {MoO_6} octahedra (dark blue), all of which are linked the central polyhedron through edge sharing.[37]

Solutions of Mo-132a and Mo-132b are brown, and mainly absorb at about 450 nm. They are stable in solution, and are capable of encapsulating certain guest species within the hollow center. This opening is a nanometer sized cavity and contains the ligands (Fig. 6), while the outer edges have a high electron density. For Mo-132b, having the divalent sulfate ligands within the cavity means that the charge density increases from the outside of the sphere to the inner ligands.[20,22,30,33,35,36]

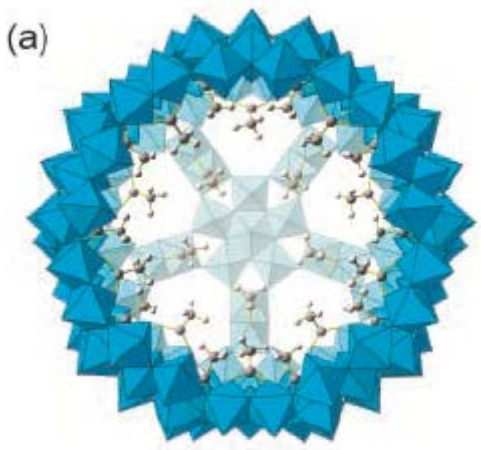

Fig. 6: Polyhedral representation of Mo-132a, where the internal acetate ligands are represented as ball-and-stick figures.[38]

1.4.2 Mo-154: the "Big Wheel"

The "big wheel" was first identified in 1995 and the Mo-154 type wheels have since been recognized as being one of the main components in molybdenum blue (where Mo-154 indicates that there are 154 molybdenum centers present in the cluster).[39,40] It was one of the first structures evolved beyond the molecular (micro) scale, and into the mesoscopic scale, i.e., between the macro and micro regimes.[41] When Mo-154 is synthesized, not all of the molybdenum centers are reduced to Mo^{V}, making it a mixed-valent (Mo^{V}/Mo^{VI}) diamagnetic cluster with the $(NH_4)_{28}\left[Mo_{154}(NO)_{14}O_{448}H_{14}(H_2O)_{70}\right]\cdot 350\ H_2O$ (Mo-154), making the charge on the wheel itself -28.[18,22,39] It contains 140 MoO_6 octahedra and 14 MoO_6(NO) pentagonal bipyramids.[39] It is a tetradecamer with approximate D_{7d} symmetry when the hydrogen atoms are not taken into account.[21]

Like the Mo-132 Keplerates, the wheel can be considered to be made up of $\{Mo_{11}\}_n$ units, where for the big wheel n=14 and for the Keplerates n=12. It could also be thought of as being constructed from 14 each of $\{Mo_8\}$, $\{Mo_2\}$, and $\{Mo_1\}$ units (Fig. 7, Fig. 9).[16-18,21,22] The

{Mo_{11}} unit contains both Mo^{V} and Mo^{VI} centers, giving the motif C_S symmetry rather than fivefold symmetry (Fig. 8). The {Mo_8} unit is contained within the {Mo_{11}} motif, where three of the outer molybdenum octahedra present in the {Mo_{11}} motif are missing in the {Mo_8} motif.[22] A solution of Mo-154 has an intense blue color, which has been attributed to inter-valence charge transfer (IVCT) transitions between the Mo^{V} and Mo^{VI} centers that results in a band in the range of 200-900 cm^{-1} in the infrared (IR) spectrum.[42]

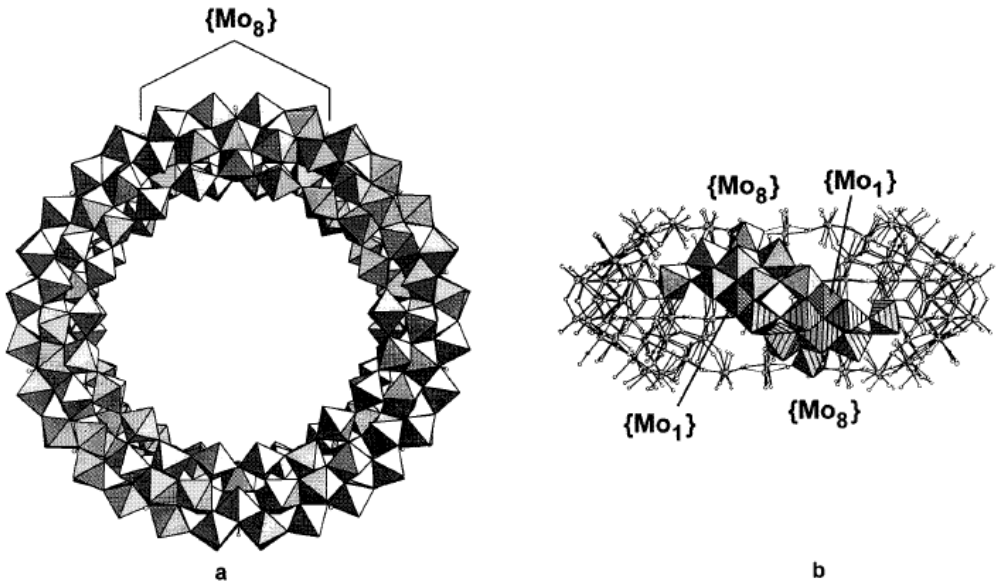

Fig. 7: (a) Polyhedral representation of Mo-154, where the {Mo_8} subunit is shown. (b) Ball-and-stick representation of a side view of Mo-154 with two {Mo_8} and {Mo_1} units emphasized through polyhedral representation.[16]

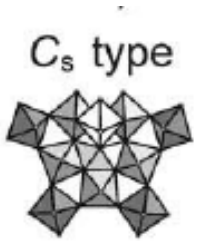

Fig. 8: Polyhedral representation of the {Mo_{11}} motif present in Mo-154. The wheel is made up of 14 of these units, each of which has C_S symmetry.[22]

The Mo-154 cluster is highly soluble due to the large number of water ligands, making both the inner and outer surfaces of the ring hydrophilic. To improve crystallization, the

concentration of electrolytes in solution must be increased in order to disrupt the hydration shell. It has a hole with a size in the nanometer range and a high surface area, explaining its high affinity for adsorbents (Fig. 9). The outer edges of the wheel have a high electron density.[20,22-24,40,42]

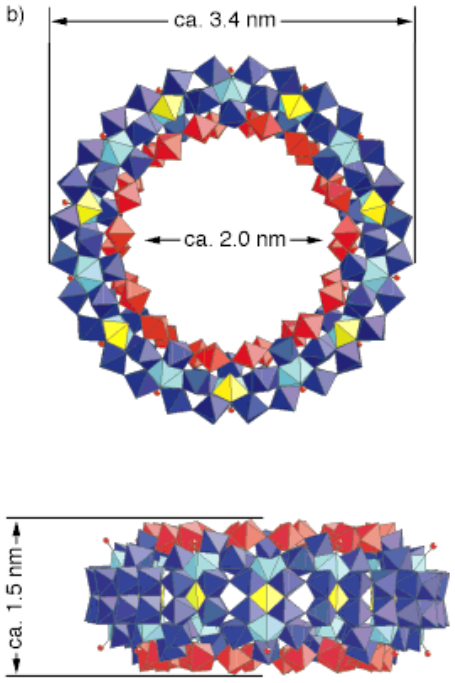

Fig. 9: Polyhedral representation of the "big wheel" Mo-154 and approximate dimensions. Shown are the different subunits that make up the structure: {Mo_8} (dark and light blue, with the light blue as the central pentagonal bipyramid and dark blue as the surrounding octahedra), {Mo_2} (red octahedra), and {Mo_1} (yellow octahedra).[18]

1.5 Literature Review

Most current research related to the nanoscale is now more focused on building larger systems from well-ordered building blocks rather than developing new nanoscopic components.[6,31] This is partially due to the fact that many of the possible applications for nanoscopic entities rely on the interaction and assembly of the nano-sized units, rather than the effects of a single nano-object.[6] Therefore, understanding aggregation tendencies at the

nanoscale is important in the design of nanomaterials for various applications, such as plasmonic sensors and drug delivery vehicles.[7]

As stated in section 1.3, oppositely charged nanoparticles will precipitate out when their charges are balanced.[14] It has been shown that this point can be reached through dilution of the solution and/or an increase in temperature. Both of these methods result in an increase in the interaction between the oppositely charged nanoparticles, leading to precipitation due to the attractive forces. In the case of dilution, the lower salt concentration leads to less screening by the ions and desorption of ions from the NP ligands, both of which serve to increase the electrostatic attraction between the oppositely charged nanoparticles. By increasing the temperature, ions desorb from the surface of the NPs, also leading to stronger electrostatic interactions.[43]

It is possible to take advantage of the electroneutrality precipitation point through the electrostatic assembly of oppositely charged nanoparticles to form large, well-defined crystals. However, it has been shown that these crystals will only form when the size distributions between the oppositely charged nanocomponents overlap, and that the crystals will be built from the particles in that overlapping region.[44]

Past research has provided the ability to synthesize nanoparticles that exhibit attractive or repulsive forces and the ability to adjust the range over which these interactions occur through the size and shape of the nano-objects. This makes electrostatic interactions useful in mediating the assembly of aggregates or crystalline structures.[7,15,44] Recently, it has been found that nanoscopic entities can be synthesized through the electrostatic assembly of nanoparticles and polyoxometalates.[31] In the present work, investigation into the concept of size-based

precipitation was expanded by observing the interaction between positively charged nanoparticles and negatively charged polyoxomolybdates.

2 Experimental Methods

2.1 Synthesis of Polyoxomolybdates

Syntheses were performed in collaboration with Stephanie Jones and Jonathan Gooch. $(NH_4)_{42}\left[Mo^{VI}_{72}Mo^{V}_{60}O_{372}(CH_3COO)_{30}(H_2O)_{72}\right]\cdot$ ca. 300 $H_2O\cdot$ ca. 10 CH_3COONH_4 (Mo-132a), $(NH_4)_{72\text{-}n}\left[\left\{(H_2O)_{81\text{-}n}+(NH_4)_n\right\}\subset\left\{\left(Mo^{VI}\right)Mo^{VI}_5O_{21}(H_2O)_6\right\}_{12}\left\{Mo^{V}_2O_4(SO_4)\right\}_{30}\right]\cdot$ca. 200 H_2O (Mo-132b), and $(NH_4)_{28}\left[Mo_{154}(NO)_{14}O_{448}H_{14}(H_2O)_{70}\right]\cdot$ 350 H_2O (Mo-154) were performed according to procedures described by Müller and coworkers.[29,30,36,39,45]

2.1.1 Synthesis of Mo-132a

Following the procedure described by Müller and coworkers[29,30,45], a solution of CH_3COONH_4 (12.5 g, 162.2 mmol) and $(NH_4)_6Mo_7O_{24}\cdot 4\ H_2O$ (5.6 g, 4.5 mmol) in 250 mL H_2O was prepared, then $N_2H_6\cdot H_2SO_4$ (0.8 mg, 6.1 mmol) was added. The solution was allowed to stir for 10 minutes, during which the solution exhibited a color change to blue-green. After the 10 minutes were complete, a 50% (v/v) solution of CH_3COOH (83 mL) was added under stirring, changing the color of the solution to green. The solution was then stored undisturbed in an open 500 mL Erlenmeyer flask for 4 days under ambient conditions, during which the solution exhibited a final color change to dark brown and red-brown crystals precipitated out. After the 4 days, the crystals were filtered out using a glass frit and washed with 90% ethanol then diethyl ether.

2.1.2 Synthesis of Mo-132b

Following the procedure described by Müller and coworkers[36], a solution of Mo-132a (2.0 g, 0.07 mmol) prepared as described in Section 2.1.1 was prepared in 160 mL H_2O. To this red-brown solution, first $(NH_4)SO_4$ (8.0 g, 60.5 mmol) then H_2SO_4 (21 mL, 2.0 M) were added under stirring. The solution was stored undisturbed in an open 400 mL beaker under ambient conditions for 2 weeks, during which brown crystals precipitated out. These crystals were filtered off using a glass frit and washed with cold 2-propanol (4 mL), then diethyl ether (4 mL) and dried using air.

2.1.3 Synthesis of Mo-154

Following the procedure described by Müller and coworkers[39], to 200 mL water, $Na_2MoO_4 \cdot 2\ H_2O$ (7.46 g, 30.8 mmol), NH_4VO_3 (1.19 g, 10.2 mmol), $NH_2OH \cdot HCl$ (12.83 g, 184.6 mmol), and HCl (3.5% v/v, 9.5 mL) were added. The mixture was stirred for 2 minutes, then the stirring was stopped while it was heated to 65°C in a 300 mL Erlenmeyer flask covered with a watchglass for 20 hours. Dark blue crystals precipitated out during this time, which were filtered out using filter paper, which was then placed in a desiccator under argon to dry.

2.2 Synthesis of Gold Nanoparticles

2.2.1 Synthesis of $Au_{1.5}$TMA ($Au_{1.5}$)

The synthesis of the 1.5 nm diameter gold core NPs functionalized with TMA was performed using a synthesis modified from the one reported by Weare, *et. al*.[46] In a 100 mL round-bottom flask, TOAB (0.160 g, 0.293 mmol) was added to a nitrogen purged toluene:water solution (6.5 mL:5.0 mL) and was allowed to stir for 5 minutes. Then $HAuCl_4 \cdot 3H_2O$ (0.100 g, 0.254 mmol) was added and the reaction was left to stir for 15 minutes. At this point, the organic

layer had turned red-orange and PPh_3 (0.232 g, 0.884 mmol) was added, turning the solution a cloudy white. After stirring 10 minutes, a solution containing excess $NaBH_4$ (0.141 g, 3.73 mmol in 10 mL water) was slowly added under high stirring. The reaction bubbled and the organic layer turned dark purple. The reaction was allowed to stir for 3 hours, after which the aqueous layer was discarded and the organic layer was dried under argon, resulting in a dark brown-black solid.

The solid was washed with hexanes, a solution of $NaNO_2$ (6 g, 87.0 mmol in 10 mL water), and a methanol:water solution (3 mL:2 mL) to remove the phase-transfer agent (TOAB), undesired byproducts, and excess reagents. After drying, DCM (6.0 mL) was added and sonicated to ensure the dissolution of the solid. The solution was split into three vials (2 mL each), and 200 µL of TMA was added (5 mM in EtOH). The vials were covered and left to stir for an hour, then 2 mL of water was added to each vial. The vials were covered again and left to stir overnight, during which the nanoparticles transferred to the aqueous layer. The vials were combined, sonicated for 30 seconds, and then centrifuged for 5 minutes at 4400 rpm. The organic layer was removed and discarded, then the aqueous layer was washed twice with DCM, repeating the sonication and centrifugation before discarding the organic layer. The $Au_{1.5}$TMA ($Au_{1.5}$) nanoparticles were stored at 4°C.

Thermogravimetric analysis (TGA) was used to determine the number of TMA ligands on the NPs, and therefore the size, as well as the concentration of the solutions used. From the number of ligands on the NPs, the charge could also be found, typically being between +36 and +42. For simplicity, this charge shall be referred to as ≈42. Further descriptions involving the interpretation of TGA results can be found in Appendix B.

2.2.2 Synthesis of $Au_{4.5}$TMA ($Au_{4.5}$)

The synthesis of the 4.5 nm diameter gold core NPs functionalized with TMA was performed using a synthesis modified from the one described by Maye, *et. al*.[47] After rinsing a 100 mL round-bottom flask and stir bar with toluene, toluene (16 mL) and TOAB (0.278 g, 0.508 mmol) were allowed to stir. A solution of $HAuCl_4 \cdot 3H_2O$ (0.040 g, 0.10 mmol in 10 mL water) was prepared and added after 15 minutes, causing the organic layer to turn dark red-orange. After 30 additional minutes of stirring, the layers were separated and the aqueous layer discarded. A solution containing excess $NaBH_4$ (0.038 g, 1.0 mmol in 20 mL H_2O) was added dropwise to the organic layer until the toluene layer turned dark purple. The round-bottom flask was covered and left to stir for 2 hours, after which the layers were separated and the aqueous layer discarded.

The toluene layer was split among 4 vials (4 mL each), and 400 µL of TMA (5 mM in EtOH) was added to each vial. The vials were covered, then left to stir overnight. The dark precipitate that had formed was separated out by centrifuging the vials for 3 minutes at 4400 rpm and decanting the toluene off. The precipitate was washed twice with ethyl acetate, sonicated for 30 seconds, and then centrifuged for 3 minutes at 4400 rpm. The ethyl acetate was decanted off and the precipitate dried under argon, then dissolved in a solution of HCl (3 mL each, pH 2). The $Au_{4.5}$TMA nanoparticles were stored at 4°C. Transmission electron microscopy was used to characterize the size of the nanoparticles. From the size, the number of ligands per NP could be calculated and therefore the charge on the NP could be found. Typically the charge would be approximately +420.

2.3 Sample Preparation and Analysis

In a typical experiment, 1 mL aliquots of diluted NPs of one size were added to snap tubes, then aliquots of one type of POM solution were added to the different snap tubes to result in different molar ratios between the NPs and POMs. Precipitation at one of the ratios (r_e, point of electroneutrality in the zeta potential measurements) would usually occur within 5 minutes. Zeta potential, DLS, and UV-Vis measurements and would then be taken. A typical concentration of the diluted NPs for $Au_{1.5}$ would be 5 μM and for $Au_{4.5}$ would be 0.05 μM.

2.4 Instrumentation

2.4.1 Zeta Potential and Dynamic Light Scattering (DLS)

Both the zeta potential and DLS measurements were performed on a Malvern Zetasizer ZS. Zeta potential measurements were made over the range of -200 mV to +200 mV at an effective voltage of 150 mV using a folded capillary cell to contain the sample. DLS measurements were made using a 173° backscatter in a low volume polystyrene cell. The samples used in the zeta potential and DLS measurements were the mixtures of NPs and POMs described in Section 2.3.

2.4.2 Ultraviolet-Visible Spectroscopy (UV-Vis)

A Varian Cary 50 spectrophotometer was used to collect UV-Vis data at a scan rate of 3000 nm/min over a range of 300-800 nm using a baseline correction. The samples were placed in 1 mL glass cuvettes, and were the same samples used in zeta potential and DLS whose preparation is described in Section 2.3.

2.4.3 Thermogravimetric Analysis (TGA)

A Perkin Elmer Pyris1 TGA was used to collect TGA data with the samples purged under nitrogen gas and heated at a rate of 10°C/min. Before the analyses were performed, the samples were dropcast and dried. The samples used were the $Au_{1.5}$ NPs whose synthesis was described in Section 2.2.1. All TGA experiments were performed by Jonathan Gooch in Dr. Zubieta's group. A representative TGA weight loss plot can be found in Appendix B.

2.4.4 Transmission Electron Microscopy (TEM)

A JEOL 2000EX operated by the SUNY-ESF N.C. Brown Center for Ultrastructure Studies was used to perform TEM measurements. It was run with a tungsten filament at 100 kV. The samples with populations of at least 100 counts were analyzed using ImageJ software. The samples used were the $Au_{4.5}$ NPs whose synthesis was described in Section 2.2.2. TEM experiments were performed by Rebeka Alam.

3 Results and Discussion

3.1 Keplerates and AuTMA Studies

3.1.1 Mo-132a and $Au_{1.5}$TMA

For the assembly between Mo-132a and $Au_{1.5}$, r = [Mo-132a]:[$Au_{1.5}$] mole ratios between 0:1 and 5:1 were studied. The brown solution of $Au_{1.5}$ grew darker upon addition of the brown Mo-132a until precipitation occurred at $r_e \approx 1$, at which point all color had left the solution to form brown aggregates. These solutions were then analyzed using zeta potential and UV-Vis. DLS studies were attempted, however the results were inconsistent, possibly due to the polydispersity of the samples caused by the aggregating particles. The zeta potential studies were

performed in collaboration with Jonathan Gooch. A set of representative zeta potential results is shown in Fig. 10.

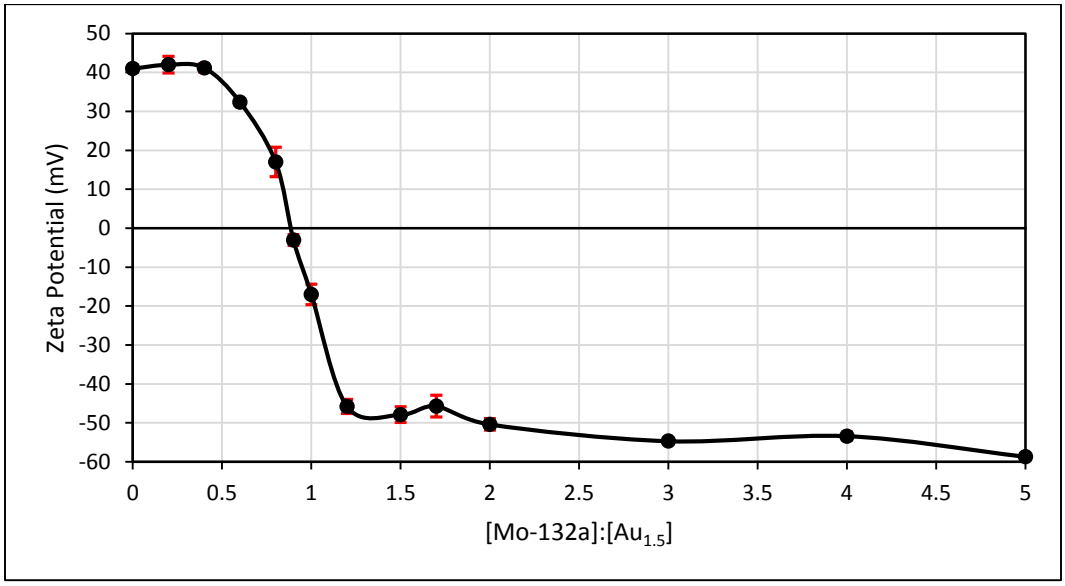

Fig. 10: A representative set of zeta potential results in the assembly of Mo-132a and $Au_{1.5}$. The red error bars shown represent the standard deviation of the measurements taken at that ratio. The precipitation point corresponded to the point of electroneutrality between the NPs and POMs observed in the zeta potential results at $r_e \approx 1$.

The zeta potential remained relatively constant before the precipitation point, then dropped drastically near the precipitation point and ratio of electroneutrality (r_e) and leveled out to a near constant value at higher values of r. This general shape of the zeta potential curve is consistent with previous studies into the electrostatic assembly of both oppositely charged nanoparticles[14,15] as well as NPs and Keplerates[31]. The ratio at which precipitation was observed corresponded to the point of electroneutrality, $r_e \approx 1$, in the zeta potential results. This ratio is in agreement with the point of charge balance between the ≈42 charged $Au_{1.5}$ and the -42 Mo-132a, indicating that this assembly may follow the tendencies of oppositely charged nanoparticles.

The UV-Vis spectra monitoring the assembly are shown in Fig. 11, with the faint SPR band centered at about λ_{max} = 520 nm. Interestingly, the absorbance bands increase as more Mo-132a is added, and drop only near the point of precipitation and electroneutrality. Consistent with

the results published by Gooch, *et. al.*,[31] the loss of the SPR band in the absorption spectra at higher r is attributed to a combination of the screening of the $Au_{1.5}$ by the Mo-132a and the aggregation and precipitation out of solution of both the NP and POM. However, the increase in absorbance at the lower ratios was not observed in the previously reported study. This can be attributed to the fact that the SPR band for $Au_{1.5}$ is much less pronounced due to its size of less than 2 nm,[46] allowing for the absorption band of Mo-132a at 450 nm to begin to be seen and to add to the absorption spectra as more POM was added as well as the darkening of the solution.[29,30,45]

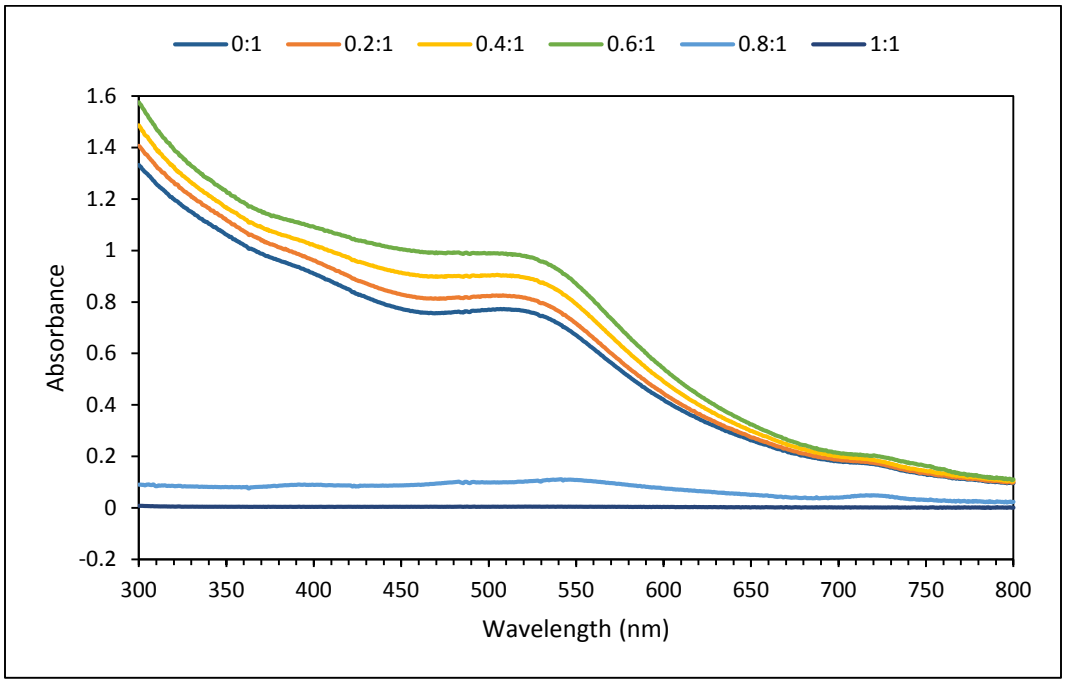

Fig. 11: Absorbance spectra monitoring the assembly of $Au_{1.5}$ and Mo-132a. [Mo-132a]:[$Au_{1.5}$] mole ratios up to $r_e \approx 1$ are shown. The small band centered at about 520 nm is the SPR band for $Au_{1.5}$.

3.1.2 Mo-132b and $Au_{1.5}$TMA

For comparison, the assembly of $Au_{1.5}$ and Mo-132b was also studied using [Mo-132b]:[$Au_{1.5}$] mole ratios between 0:1 and 2.2:1 were studied. The brown solution of $Au_{1.5}$ grew darker upon addition of the red-brown Mo-132b until precipitation occurred at $r_e \approx 0.6$, at which point the solution became clear at the precipitation of brown aggregates. These solutions

were analyzed using zeta potential and UV-Vis. DLS studies were attempted, however it appeared that the formation of the aggregates made the solutions too polydisperse for analysis. The zeta potential studies were performed in collaboration with Jonathan Gooch, with representative zeta potential results shown in Fig. 12.

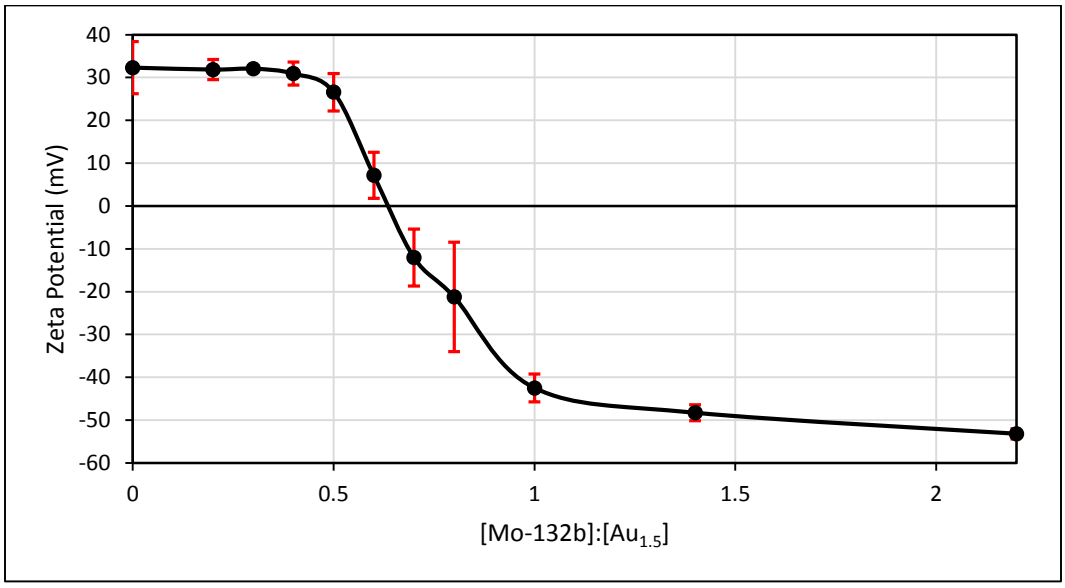

Fig. 12: A set of representative zeta potential results in the assembly of Mo-132b and $Au_{1.5}$. The red error bars shown represent the standard deviation of the measurements taken at that ratio. The precipitation point corresponded to the point of electroneutrality between the NPs and POMs observed in the zeta potential results at $r_e \approx 0.6$.

The overall shape of the curve is quite similar to the zeta potential results in the assembly of $Au_{1.5}$ and Mo-132a, as well as previous studies.[14,15,31] The precipitation point occurred at $r_e \approx 0.6$ observed in the zeta potential results. This point also corresponds to the point of electroneutrality between the NP with a charge of ≈42 and the -72 Mo-132b.

The UV-Vis spectra monitoring the assembly of $Au_{1.5}$ and Mo-132b are shown in Fig. 13. Similar to the assembly involving Mo-132a, as more Mo-132b is added the absorbance increases then drops only near the point of precipitation and electroneutrality. Again, the loss of the SPR band at higher r is attributed to both the screening of the $Au_{1.5}$ by the Mo-132b and the aggregation and precipitation out of solution of both entities. The increase in the absorption band

can be attributed to the characteristic Mo-132b band at 450 nm beginning to be seen as more POM was added and the solution darkened.[29,30,45]

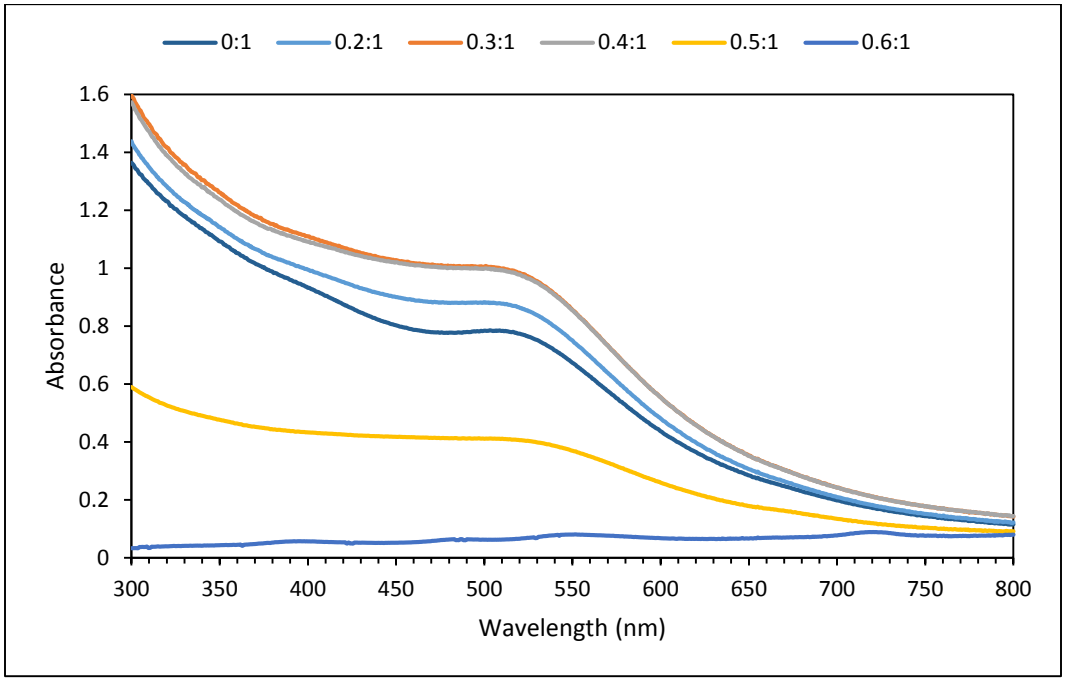

Fig. 13: Absorbance spectra monitoring the assembly of $Au_{1.5}$ and Mo-132b. [Mo-132b]:[$Au_{1.5}$] mole ratios up to $r_e \approx 0.6$ are shown. The small band centered at about 520 nm is the SPR band for $Au_{1.5}$.

In the results reported by Gooch, *et. al.*[31], which studied the assembly of Mo-132a and Mo-132b with $Au_{4.5}$, different results were observed. The literature results showed that r_e for the assembly between the more negatively charged Mo-132b and $Au_{4.5}$ ($r_e \approx 14$) was higher than that of Mo-132a and $Au_{4.5}$ ($r_e \approx 10$). These results appeared counterintuitive, since it would be expected that a smaller amount of the more negatively charged Mo-132b would be needed to balance the positive charge on the NPs. This observation was explained with two main arguments: (1) as the Keplerates and NPs came together, their electric double layers and counterions could have interacted in such a way that the new double layers forming around the aggregates would affect the zeta potential values observed (Fig. 14), and (2) the higher charge on Mo-132b would result in a stronger attraction between the NH_4^+ counterions and the sphere,

which would screen the attractive nature between Mo-132b and the NPs to a greater extent than the Mo-132a counterions. This decreased attraction between Mo-132b and $Au_{4.5}$ could have led to the higher r_e value observed.[31]

In the present work involving the smaller and less charged $Au_{1.5}$, the opposite trend was observed. This seemed sensible since, as stated before, it would be expected that less of the more negatively charged Mo-132b would be needed to achieve charge balance. Also, the results of both Keplerates precipitating out with $Au_{1.5}$ at the point of charge balance between the NPs and POMs indicated that the assembly of $Au_{1.5}$ and Keplerates operated in a similar manner to that of oppositely charged NPs. Overall, these results indicate that the size of the nanoparticle affects the point of aggregation.

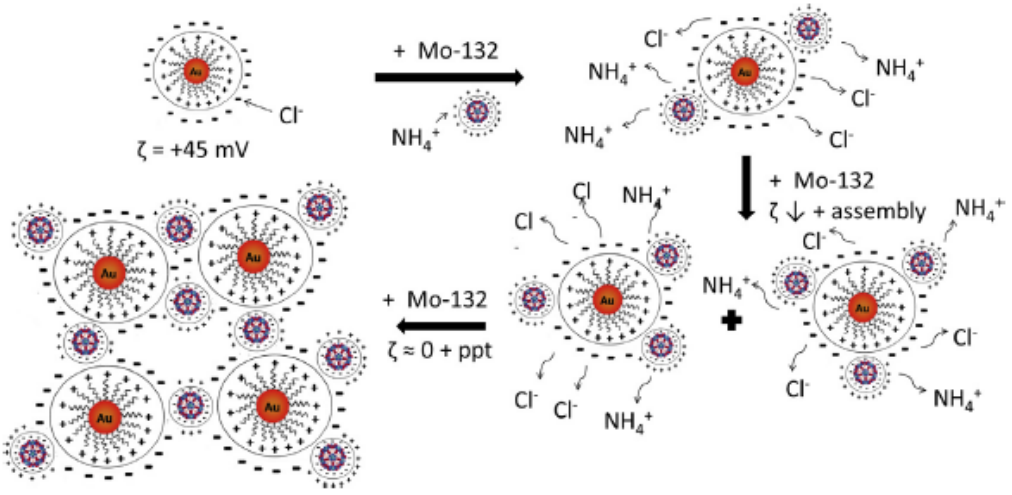

Fig. 14: Diagram showing how the layers of counterions surrounding the Keplerates and the NPs would have been disturbed as the assembly progressed. This could have affected the zeta potential results.[31]

3.2 Mo-154 and AuTMA Studies

3.2.1 Mo-154 and $Au_{1.5}$TMA

In the assembly of $Au_{1.5}$ and Mo-154 was studied using [Mo-154]:[$Au_{1.5}$] mole ratios between 0:1 and 0.9:1 were studied through zeta potential, DLS, and UV-Vis. DLS and UV-Vis

measurements were performed in collaboration with Jonathan Gooch. The brown solution of $Au_{1.5}$ grew darker upon addition of the dark blue Mo-154 until the precipitation point of $r_e \approx 0.4$, when the solution lost all color and brown aggregates formed. Representative zeta potential results are shown in Fig. 15, where the general shape of the curve is similar to those reported in previous studies.[14,15,31]

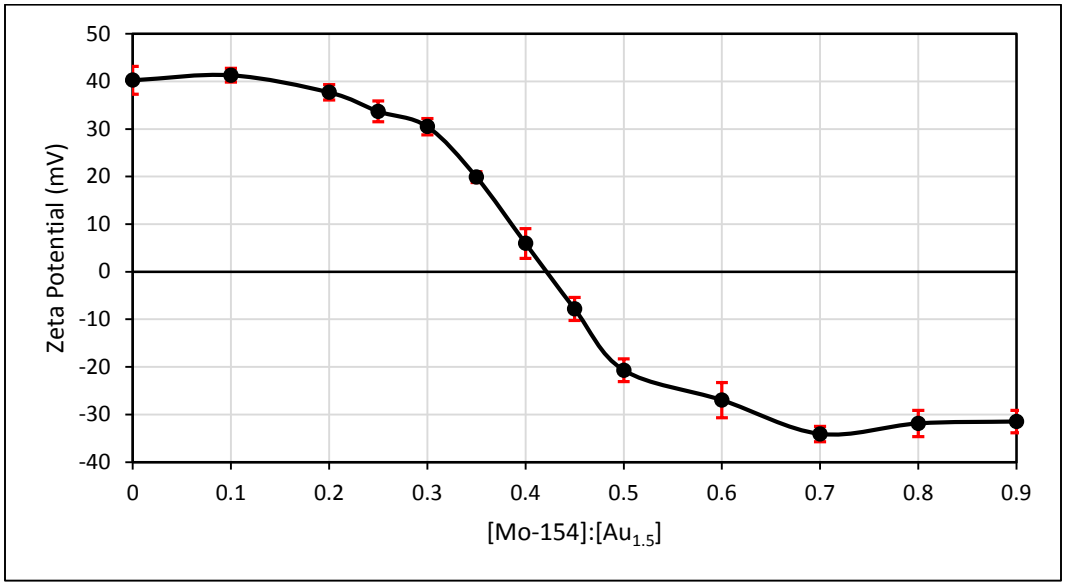

Fig. 15: A set of representative zeta potential results in the assembly of Mo-154 and $Au_{1.5}$. The red error bars shown represent the standard deviation of the measurements taken at that ratio. The precipitation point corresponded to the isoelectric point observed in the zeta potential results at $r_e \approx 0.4$.

The UV-Vis absorption spectra up to r_e are shown in Fig. 16, with the SPR band for $Au_{1.5}$ being centered at about λ_{max} = 520 nm. Consistent with the previous studies reported here, as r_e is approached and aggregates begin to form, the absorption bands decrease, likely due to both the screening of the NPs by the addition of the POM and the formation and precipitation of aggregates. The spectra for r values between 0.2 and 0.3 lie above $Au_{1.5}$ due to the fact that the addition of Mo-154 darkened the solution and Mo-154 absorbs around the SPR band between about 500-900 nm due to IVCT between Mo^{V} and Mo^{VI} centers.[40]

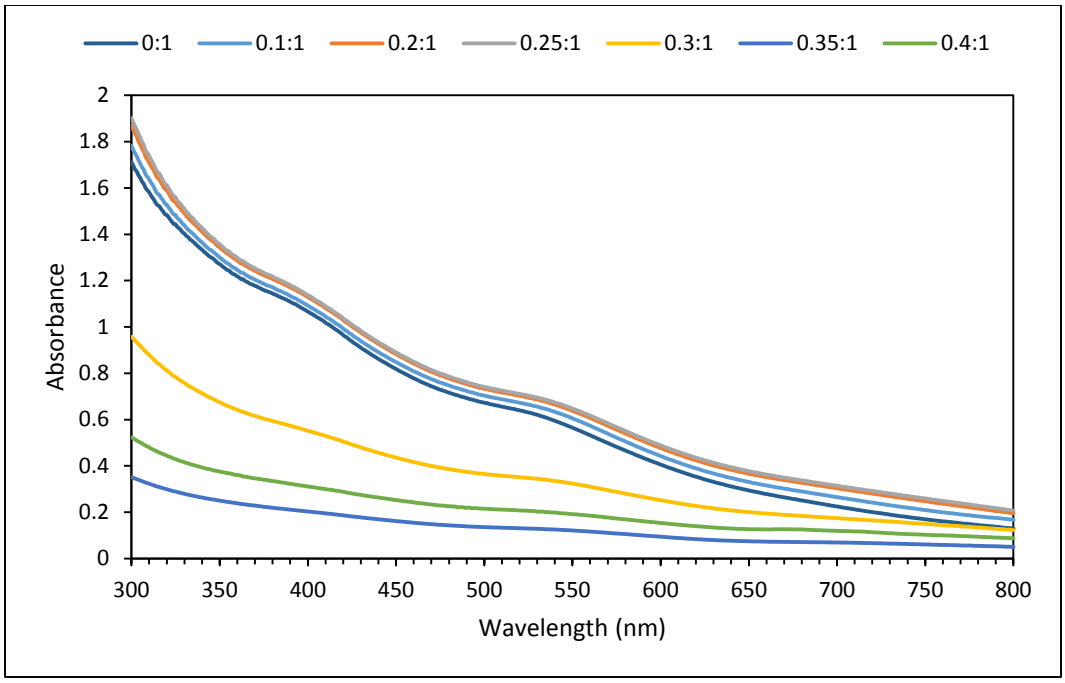

Fig. 16: Absorbance spectra monitoring the assembly of $Au_{1.5}$ and Mo-154. [Mo 154]:[$Au_{1.5}$] mole ratios up to $r_e \approx 0.4$ are shown. The small band centered at about 520 nm is the SPR band for $Au_{1.5}$.

A comparison of the UV-Vis and DLS measurements to show how the hydrodynamic diameter of the aggregates (D_h) increases while the absorbance maximum decreases at increasing r can be found in Fig. 17. Similar to the zeta potential results, the UV-Vis maxima remained relatively constant until the precipitation point was approached, when a sudden drop occurred. This loss of the SPR band is consistent with the formation of aggregates observed and the precipitation of both the Mo-154 and $Au_{1.5}$ from solution. The UV-Vis maxima reported here have taken into account the different initial absorbances.

Unlike the studies performed with $Au_{1.5}$ and the Keplerates, the ratio at which precipitation occurred does not correspond to the point of charge balance between the -28 Mo-154 and the ≈42 AuNP. From charge balance considerations alone, it would be expected that a greater amount of the less negatively charged Mo-154 would be needed than either of the Mo-

132 POMs to balance out the charges on the NP. Therefore, the expected r_e value based on the trend observed in the assembly of the Keplerates and $Au_{1.5}$ would be $r_e \approx 1.5$.

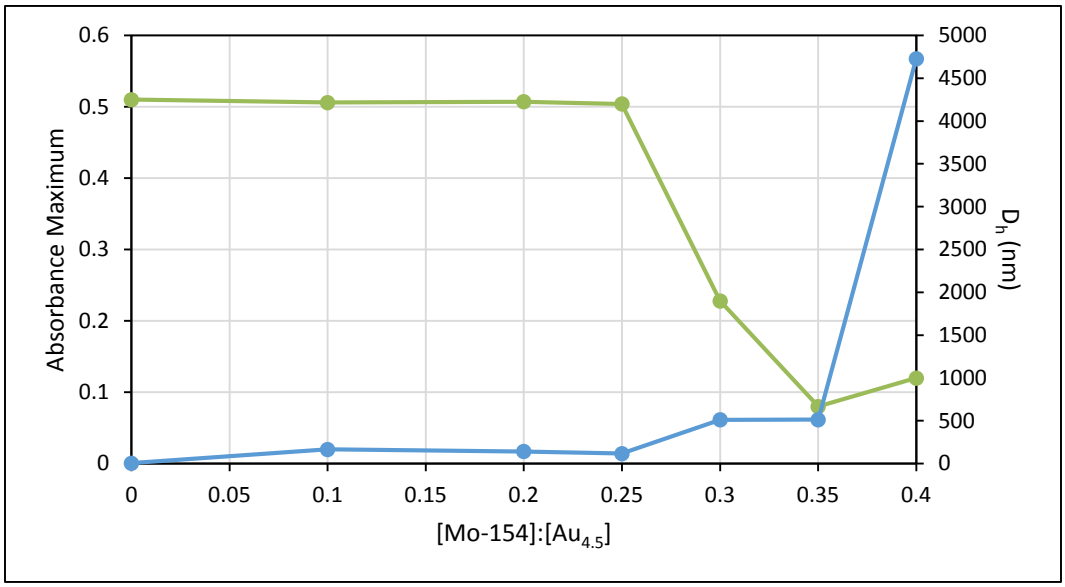

Fig. 17: Plot showing the change in the absorbance maximum corresponding to the SPR band until r_e has been reached (green), as well as the change in D_h of the aggregates (blue).

There are two main possible explanations for why this is occurring. (1) With the Keplerates, the screening of the inner charged ligands by the actual structure of the sphere could reduce the attraction between the Mo-132 and $Au_{1.5}$. In the case of the wheel, the high electron density on the edges[20,22] could mean that there is a higher level of attraction between Mo-154 and $Au_{1.5}$ than the Keplerates due to the lack of screening. (2) The cavity in the center is large enough to allow ions to pass through, meaning that when the Mo-154 approaches the $Au_{1.5}$, it may be better able to penetrate the electric double layer. The ions that make up the double layer could pass through the wheel, rather than being forced to pass around the sphere of the Keplerate. Essentially this could let the Mo-154 and the NPs to aggregate more effectively, and thus allow for a lower precipitation point.

3.2.2 Mo-154 and $Au_{4.5}$TMA

The assembly of $Au_{4.5}$ with Mo-154 was studied over the range of r = [Mo-154]:[$Au_{4.5}$] = 0:1 to 30:1 mole ratios. The red solution of $Au_{4.5}$ turned purple as the blue solution of Mo-154 was added until precipitation occurred at $r_e \approx 8$, when the solution became clear and purple aggregates precipitated out. The system was monitored using zeta potential measurements (Fig. 18). Much like the preceding studies reported here, the overall shape of the curve is consistent with those results and those reported in literature.[14,15,31]

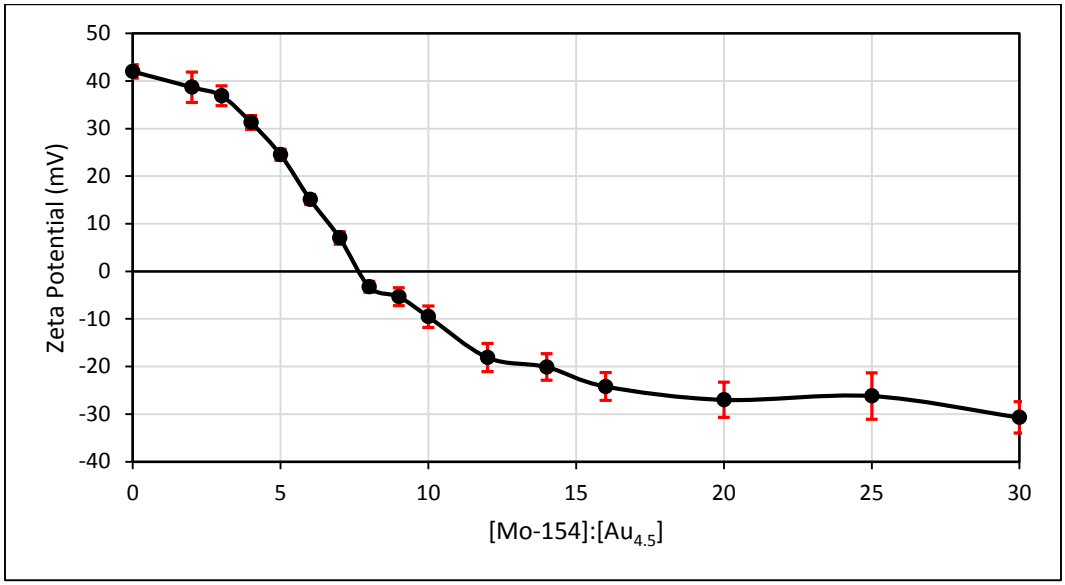

Fig. 18: A set of representative zeta potential results in the assembly of Mo-154 and $Au_{4.5}$. The red error bars shown represent the standard deviation of the measurements taken at that ratio. The precipitation point corresponded to the isoelectric point observed in the zeta potential results at $r_e \approx 8$.

This system follows the trend reported by Gooch, *et. al.* in that the point of electroneutrality occurs at a lower ratio than what would be anticipated based purely on the charges of the NPs and POMs. Similar to that study, the less negatively charged Mo-154 (-28) precipitated out at a lower ratio than either of the Keplerates. This indicates that the same arguments reported there would apply to this system. The interaction of the electric double layers

of both the NPs and the POMs could affect the zeta potential values, and the shielding caused by the counterions could lead to a decreased attraction between the two types of entities.[31]

The UV-Vis spectra monitoring the assembly between $Au_{4.5}$ and Mo-154 are shown in Fig. 19. The absorbance continuously decreases as r increases, consistent with previously published results involving $Au_{4.5}$ and Mo-132 Keplerates. Also consistent with previously published studies, a slight red-shift is observed in the SPR band as r increases, which is attributed to the formation of aggregates.[3,5,7,14,15,31] Unlike the UV-Vis results involving $Au_{1.5}$, addition of the Mo-154 at lower ratios did not lead to an increase in absorption. This is attributed to the more pronounced SPR band with a much higher extinction coefficient masking any absorption due to the POM, consistent with the previously reported study involving $Au_{4.5}$ and Mo-132 Keplerates.[31]

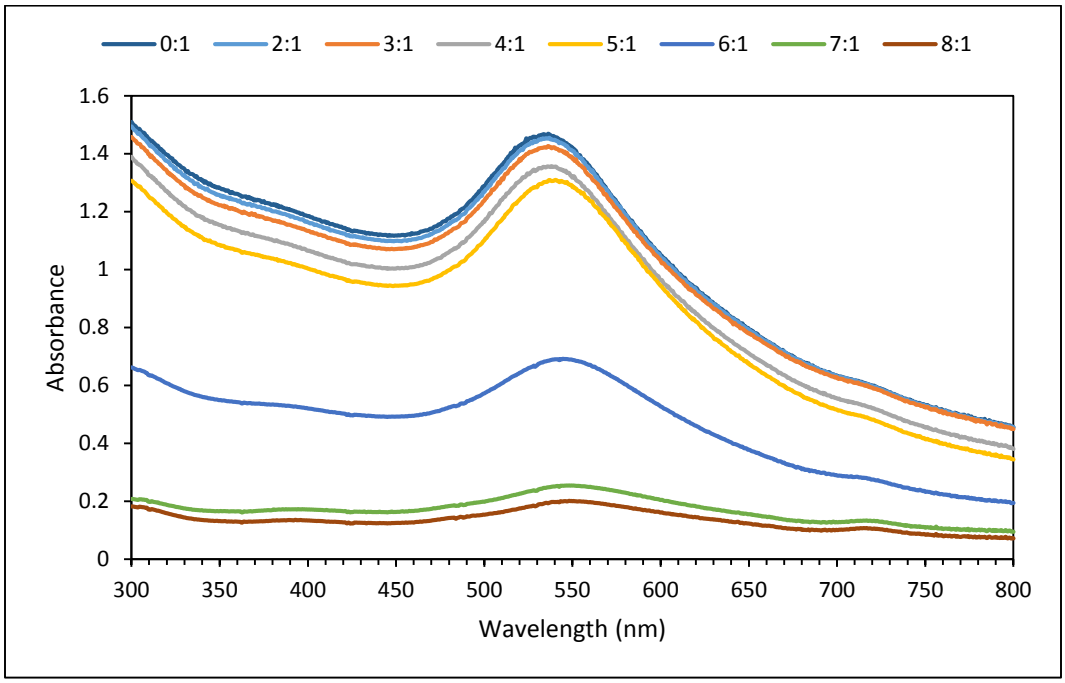

Fig. 19: Absorbance spectra monitoring the assembly of $Au_{4.5}$ and Mo-154. [Mo-154]:[$Au_{4.5}$] mole ratios up to $r_e \approx 8$ are shown. The band centered at about 530 nm is the SPR band for $Au_{4.5}$.

A summary of the results found in the present work, as well as those published by Gooch, *et. al.* for comparison, are shown in Table 1.[31] In the case of the assembly system involving $Au_{4.5}$

and Mo-154, the results were consistent with those published previously. The trend observed was counterintuitive to the studies involving oppositely charged nanoparticles, but the trend was consistent within the studies involving $Au_{4.5}$. Therefore, the arguments used by Gooch. *et. al.* involving the interaction of the two electric double layers and the shielding of the adsorbed counterions on the POMs would be applicable in explaining these observations.[31] In the studies involving $Au_{1.5}$, the results did not show a consistent trend based on the charges of the POMs, indicating that some factor other than charge plays a role in the point of precipitation. Although, the precipitation points for Mo-132a and Mo-132b follow the trend observed when oppositely charged NPs are combined in solution, where their precipitation ratios occur approximately where the charges on the $Au_{1.5}$ and Mo-132 are balanced. This could indicate that the Mo-154 is the outlier, and therefore that the shape of the POM plays a larger role in the assembly process with $Au_{1.5}$ than $Au_{4.5}$. Further studies would be required to determine the level of dependence that shape and charge have on the electrostatic assembly of AuNPs and POMs.

Table 1: Summary of the r_e^* values at which precipitation occurred in each of the systems studied in the present work, as well as the results published by Gooch, *et. al* for comparison.[31] The POMs are displayed by increasing negative charge: Mo-154 (-28), Mo-132a (-42), and Mo-132b (-72).

	Mo-154	**Mo-132a**	**Mo-132b**
$Au_{1.5}$	0.4	1	0.6
$Au_{4.5}$	8	10[31]	14[31]

4 Conclusions and Future Work

In the present work, the electrostatic assembly of cationic AuNPs with anionic POMs were investigated to further expand on both the work published by Gooch, *et. al* and studies into the interaction of oppositely charged nanoparticles. The NPs used were functionalized with N,N,N-trimethyl(11-mercaptoundecyl)ammonium chloride, with gold cores of approximately 1.5

nm and 4.5 nm. The POMs used were the Mo-154 “Big Wheel” and Mo-132 Keplerates containing either acetate or sulfate ligands. The assembly process was monitored through zeta potential and UV-Vis, and DLS measurements were attempted. The zeta potential and UV-Vis results indicated that successful assembly between the oppositely charged entities was successful, however the DLS measurements were inconclusive, most likely due to the polydispersity of the aggregates caused by the assembly process. The precipitation from solution of the NPs and POMs occurred at the point of electroneutrality, as measured by zeta potential. The UV-Vis results showed the loss of the SPR band for the AuNPs as aggregation and precipitation occurred. In all of the studies involving $Au_{1.5}$, the absorption increased as more of the POM was added, then the absorption bands dropped as r_e was approached. This was not observed in the study performed here involving Mo-154 and $Au_{4.5,}$ or those previously reported. This was attributed to the more pronounced SPR band for $Au_{4.5}$ masking the absorption band characteristic of Mo-154, consistent with the previously reported studies involving Mo-132 Keplerates.

Including the previously reported results involving $Au_{4.5}$ and Mo-132 Keplerates, a consistent trend was observed across the Mo-132 and Mo-154 POMs and $Au_{4.5}$. The ratio at which electroneutrality and precipitation occurred increased from $r_e \approx 8$ (Mo-154), $r_e \approx 10$ (Mo-132a), to $r_e \approx 14$ (Mo-132b) as the charge on the POMs became more negative. Although these results do not correspond to the trend observed for oppositely charged nanoparticles, where they will only precipitate out when the charges on the NPs are balanced, they do form a consistent trend. These counterintuitive results were justified by Gooch, *et. al*. by explaining how the interaction of the two species’ electric double layers and the stronger attraction of the POMs counterions as the negative charge increases would impact the results. The interaction of the

double layers of both the AuNPs and the POMs could affect the zeta potential values, and the increased shielding of the POMs by the adsorbed counterions as the POMs become more negatively charged could lead to a decreased attraction between the two types of entities.

In the studies involving $Au_{1.5}$ and the Mo-132 Keplerates, it appeared that ratios of $r_e \approx 1$ (Mo-132a) and $r_e \approx 0.6$ (Mo-132b) at which electroneutrality and precipitation occurred correspond to the ratios at which the charges on the NPs and Keplerates are balanced. This indicates that for these spherical entities, they follow the trends reported when oppositely charged nanoparticles are combined. However, the $r_e \approx 0.4$ observed when $Au_{1.5}$ and Mo-154 are combined does not correspond to the point of charge balance between the NPs and POMs. Therefore, the differing shapes of the Mo-154 wheel and the Mo-132 spheres appears to be affecting how these entities interact and precipitate. This could possibly be due to the high electron density on the outer edges of the Mo-154 leading to a higher level of attraction between the AuNPs and POMs and lowering the observed r_e value, or the wheel shape of the Mo-154 and its hollow center could allow it to better penetrate the electric double layer of the $Au_{1.5}$.

Since the trends observed for $Au_{1.5}$ are different than those observed for $Au_{4.5}$, it is likely that the different sizes of the NPs also influence how these types of entities interact. Essentially, these results indicate that both the charges on the POMs and their shape have an impact on how these species interact with nanoparticles, and that the size of the NPs affect how they interact with polyoxomolybdates. Further studies should be performed to investigate what role these factors play in the electrostatic assembly of anionic polyoxomolybdates and cationic gold nanoparticles. Possible avenues of this research could include different sized nanoparticles or additional non-spherical POMs.

5 References

1. Daniel, M.; Astruc, D. Gold Nanoparticles: Assembly, Supramolecular Chemistry, Quantum-Size-Related Properties, and Applications toward Biology, Catalysis, and Nanotechnology. *Chem. Rev.* **2004**, *104*, 293-346.
2. Bishop, K. J. M.; Grzybowski, B. A. "Nanoions": Fundamental Properties and Analytical Applications of Charged Nanoparticles. *ChemPhysChem* **2007**, *8*, 2171-2176.
3. Voliani, V. *Update on Gold Nanoparticles : From Cathedral Windows to Nanomedicine;* iSmithers Rapra Pub: Shrewsbury, 2013; , pp 148.
4. Uzun, O.; Hu, Y.; Verma, A.; Chen, S.; Centrone, A.; Stellacci, F. Water-soluble amphiphilic gold nanoparticles with structured ligand shells. *Chem. Commun.* **2008**, 196-198.
5. Sperling, R. A.; Rivera Gil, P.; Zhang, F.; Zanella, M.; Parak, W. J. Biological applications of gold nanoparticles. *Chem. Soc. Rev.* **2008**, *37*, 1896-1908.
6. Bishop, K. J. M.; Wilmer, C. E.; Soh, S.; Grzybowski, B. A. Nanoscale Forces and Their Uses in Self-Assembly. *Small* **2009**, *5*, 1600-1630.
7. Wang, D.; Kowalczyk, B.; Lagzi, I.; Grzybowski, B. A. Bistability and Hysteresis During Aggregation of Charged Nanoparticles. *J. Phys. Chem. Lett.* **2010**, *1*, 1459-1462.
8. Grzybowski, B. A. Charged nanoparticles crystallizing and controlling crystallization: from coatings to nanoparticle surfactants to chemical amplifiers. *CrystEngComm* **2014**, *16*, 9368-9380.
9. Olson, E. Zeta potential and colloid chemistry. *Journal of GXP Compliance* **2012**, *16*, 81-96.
10. Doane, T. L.; Chuang, C.; Hill, R. J.; Burda, C. Nanoparticle ζ-Potentials. *Acc. Chem. Res.* **2012**, *45*, 317-326.
11. Laaksonen, T.; Ahonen, P.; Johans, C.; Kontturi, K. Stability and Electrostatics of Mercaptoundecanoic Acid-Capped Gold Nanoparticles with Varying Counterion Size. *ChemPhysChem* **2006**, *7*, 2143-2149.
12. Lyklema, J. Molecular interpretation of electrokinetic potentials. *Curr. Opin. Colloid Interface Sci.* **2010**, *15*, 125-130.
13. Attard, P. Recent advances in the electric double layer in colloid science. *Curr. Opin. Colloid Interface Sci.* **2001**, *6*, 366-371.
14. Kalsin, A. M.; Kowalczyk, B.; Smoukov, S. K.; Klajn, R.; Grzybowski, B. A. Ionic-like behavior of oppositely charged nanoparticles. *J. Am. Chem. Soc.* **2006**, *128*, 15046-15047.
15. Walker, D. A.; Kowalczyk, B.; de la Cruz, M. O.; Grzybowski, B. A. Electrostatics at the nanoscale. *Nanoscale* **2011**, *3*, 1316-1344.
16. Müller, A.; Peters, F.; Pope, M. T.; Gatteschi, D. Polyoxometalates: Very Large Clusters-Nanoscale Magnets. *Chem. Rev.* **1998**, *98*, 239-272.

17. Cronin, L.; Beugholt, C.; Müller, A. Towards the construction of mesoscopic species with emergent and functional properties via the derivatisation of molybdenum-oxide 'Giant-Wheel' clusters. *J. Mol. Struct. : THEOCHEM* **2000**, *500*, 181-193.

18. Müller, A.; Krickemeyer, E.; Bögge, H.; Schmidtmann, M.; Beugholt, C.; Das, S. K.; Peters, F. Giant Ring-Shaped Building Blocks Linked to Form a Layered Cluster Network with Nanosized Channels: $[Mo_{124}^{VI}Mo_{28}^{V}O_{429}(\mu_3\text{-}O)_{28}H_{14}(H_2O)_{66.5}]^{16-}$. *Chem. - Eur. J.* **1999**, *5*, 1496-1502.

19. Müller, A.; Das, S. K.; Bögge, H.; Beugholt, C.; Schmidtmann, M. Assembling nanosized ring-shaped synthons to an anionic layer structure based on the synergetically induced functional complementarity of their surface-sites: $Na_{21}[Mo^{VI}_{126}Mo^{V}_{28}O_{462}H_{14}(H_2O)_{54}(H_2PO_2)_7]\cdot xH_2O$ ($x \approx 300$). *Chem. Commun.* **1999**, 1035-1036.

20. Cronin, L.; Kögerler, P.; Müller, A. Controlling Growth of Novel Solid-State Materials via Discrete Molybdenum-Oxide-Based Building Blocks as Synthons. *J. Solid State Chem.* **2000**, *152*, 57-67.

21. Müller, A.; Fenske, D.; Kögerler, P. From giant molecular clusters and precursors to solid-state structures. *Curr. Opin. Solid State Mater. Sci.* **1999**, *4*, 141-153.

22. Müller, A.; Kögerler, P.; Bögge, H. Pythagorean Harmony in the World of Metal Oxygen Clusters of the $\{Mo_{11}\}$ Type: Giant Wheels and Spheres both Based on a Pentagonal Type Unit. *Struct. Bond.* **2000**, *96*, 203-236.

23. Müller, A.; Das, S. K.; Fedin, V. P.; Krickemeyer, E.; Beugholt, C.; Bögge, H.; Schmidtmann, M.; Hauptfleisch, B. Rapid and Simple Isolation of the Crystalline Molybdenum-Blue Compounds with Discrete and Linked Nanosized Ring-Shaped Anions: $Na_{15}[Mo^{VI}_{126}Mo^{V}_{28}O_{462}H_{14}(H_2O)_{70}]_{0.5}[Mo^{VI}_{124}Mo^{V}_{28}O_{457}H_{14}(H_2O)_{68}]_{0.5}$ · ca. 400 H_2O and $Na_{22}[Mo^{VI}_{118}Mo^{V}_{28}O_{442}H_{14}(H_2O)_{58}]$ · ca. 250 H_2O. *Z. Anorg. Allg. Chem.* **1999**, *625*, 1187-1192.

24. Müller, A.; Kögerler, P. Constructing clusters from linkable units: from a giant icosahedral Keplerate to multi-functional metal-oxide based network structures. *Education in Advanced Chemistry* **2000**, *7*, 7-35.

25. Müller, A.; Roy, S.; Schmidtmann, M.; Bögge, H. Urea as '*deus ex machina*' in giant molybdenum blue type cluster synthesis: an unusual hybrid compound with perspectives for related nano, supramolecular and extended structures. *Chem. Commun.* **2002**, 2000-2002.

26. Cronin, L.; Beugholt, C.; Krickemeyer, E.; Schmidtmann, M.; Bögge, H.; Kögerler, P.; Luong, T. K. K.; Müller, A. "Molecular Symmetry Breakers" Generating Metal-Oxide-Based Nanoobject Fragments as Synthons for Complex Structures: $[\{Mo_{128}Eu_4O_{388}H_{10}(H_2O)_{81}\}_2]^{20-}$, a Giant-Cluster Dimer. *Angew. Chem.* **2002**, *114*, 2929-2932.

27. Kögerler, P.; Müller, A. Combinatorially Linkable Metal-Oxide Based Units: Perspectives for Nano, Supramolecular, and Solid-State Chemistry. In *Polyoxometalate Molecular Science;* Borrás-Almenar, J. J., Coronado, E., Müller, A. and Pope, M., Eds.; Springer: Netherlands, 2003; Vol. 98, pp 297-323.

28. Müller, A.; Roy, S. En route from the mystery of molybdenum blue via related manipulatable building blocks to aspects of materials science. *Coord. Chem. Rev.* **2003**, *245*, 153-166.

29. Cronin, L.; Diemann, E.; Müller, A. Polyoxomolybdate Clusters: Nanoscopic Wheels and Balls. In *Inorganic Experiments;* Woollins, J. D., Ed.; Wiley-VCH: Weinheim, 2003; , pp 340-346.

30. Müller, A.; Krickemeyer, E.; Bögge, H.; Schmidtmann, M.; Peters, F. Organizational Forms of Matter: An Inorganic Super Fullerene and Keplerate Based on Molybdenum Oxide. *Angew. Chem. Int. Ed.* **1998**, *37*, 3359-3363.

31. Gooch, J.; Jalan, A. A.; Jones, S.; Hine, C. R.; Alam, R.; Garai, S.; Maye, M. M.; Müller, A.; Zubieta, J. Keplerate cluster (Mo-132) mediated electrostatic assembly of nanoparticles. *J. Colloid Interface Sci.* **2014**, *432*, 144-150.

32. Müller, A.; Kögerler, P.; Dress, A. W. M. Giant metal-oxide-based spheres and their topology: from pentagonal building blocks to keplerates and unusual spin systems. *Coord. Chem. Rev.* **2001**, *222*, 193-218.

33. Müller, A.; Polarz, S.; Das, S. K.; Krickemeyer, E.; Bögge, H.; Schmidtmann, M.; Hauptfleisch, B. "Open and Shut" for Guests in Molybdenum-Oxide-Based Giant Spheres, Baskets, and Rings Containing the Pentagon as a Common Structural Element. *Angew. Chem. Int. Ed.* **1999**, *38*, 3241-3245.

34. Müller, A.; Sarkar, S.; Shah, S. Q. N.; Bögge, H.; Schmidtmann, M.; Sarkar, S.; Kögerler, P.; Hauptfleisch, B.; Trautwein, A. X.; Schünemann, V. Archimedean Synthesis and Magic Numbers: "Sizing" Giant Molybdenum-Oxide-Based Molecular Spheres of the Keplerate Type. *Angew. Chem. Int. Ed.* **1999**, *38*, 3238-3241.

35. Müller, A.; Krickemeyer, E.; Bögge, H.; Schmidtmann, M.; Botar, B.; Talismanova, M. O. Drawing Small Cations into Highly Charged Porous Nanocontainers Reveals "Water" Assembly and Related Interaction Problems. *Angew. Chem. Int. Ed.* **2003**, *42*, 2085-2090.

36. Müller, A.; Zhou, Y.; Bögge, H.; Schmidtmann, M.; Mitra, T.; Haupt, E. T. K.; Berkle, A. "Gating" the Pores of a Metal Oxide Based Capsule: After Initial Cation Uptake Subsequent Cations Are Found Hydrated and Supramolecularly Fixed above the Pores. *Angew. Chem.* **2006**, *118*, 474-479.

37. Müller, A.; Kögerler, P.; Kuhlmann, C. A variety of combinatorially linkable units as disposition:† from a giant icosahedral Keplerate to multi-functional metal–oxide based network structures. *Chem. Commun.* **1999**, 1347-1358.

38. Kurth, D. G.; Lehmann, P.; Volkmer, D.; Müller, A.; Schwahn, D. Biologically inspired polyoxometalate-surfactant composite materials. Investigations on the structures of discrete, surfactant-encapsulated clusters, monolayers, and Langmuir-Blodgett films of $(DODA)_{40}(NH_4)_2(H_2O)_n \subset Mo_{132}O_{372}(CH_3CO_2)_{30}(H_2O)_{72}]$. *J. Chem. Soc. Dalton Trans.* **2000**, 3989-3998.

39. Müller, A.; Krickemeyer, E.; Meyer, J.; Bögge, H.; Peters, F.; Plass, W.; Diemann, E.; Dillinger, S.; Nonnenbruch, F.; Randerath, M.; Menke, C. $[Mo_{154}(NO)_{14}O_{420}(OH)_{28}(H2O)_{70}]^{(25 \pm 5)-}$: A Water-Soluble Big Wheel with More than 700

Atoms and a Relative Molecular Mass of About 24000. *Angew. Chem. Int. Ed. Engl.* **1995**, *34*, 2122-2124.

40. Müller, A.; Serain, C. Soluble Molybdenum Blues- "des Pudels Kern". *Acc. Chem. Res.* **2000**, *33*, 2-10.
41. Müller, A. An Unusual Inorganic Giant Wheel with High Symmetry, 154 Metal Atoms, and a Nanosized Cavity. *Chem. Intell.* **1997**, *3*, 58.
42. Müller, A.; Meyer, J.; Krickemeyer, E.; Diemann, E. Molybdenum Blue: A 200 Year Old Mystery Unveiled. *Angew. Chem. Int. Ed. Engl.* **1996**, *35*, 1206-1208.
43. Bishop, K. J. M.; Kowalczyk, B.; Grzybowski, B. A. Precipitation of Oppositely Charged Nanoparticles by Dilution and/or Temperature Increase. *J. Phys. Chem. B* **2009**, *113*, 1413-1417.
44. Kowalczyk, B.; Kalsin, A. M.; Orlik, R.; Bishop, K. J. M.; Patashinskii, A. Z.; Mitus, A.; Grzybowski, B. A. Size Selection During Crystallization of Oppositely Charged Nanoparticles. *Chem. - Eur. J.* **2009**, *15*, 2032-2035.
45. Müller, A.; Das, S. K.; Krickemeyer, E.; Kuhlmann, C. Polyoxomolybdate clusters: Giant wheels and balls. In *Inorganic Syntheses;* Shapley, J. R., Ed.; Wiley: New York, 2004; Vol. 34, pp 191-200.
46. Weare, W. W.; Reed, S. M.; Warner, M. G.; Hutchison, J. E. Improved Synthesis of Small ($d_{CORE} \approx 1.5$ nm) Phosphine-Stabilized Gold Nanoparticles. *J. Am. Chem. Soc.* **2000**, *122*, 12890-12891.
47. Maye, M. M.; Lim, I. I.; Luo, J.; Rab, Z.; Rabinovich, D.; Liu, T.; Zhong, C. J. Mediator-template assembly of nanoparticles. *J. Am. Chem. Soc.* **2005**, *127*, 1519-1529.

Appendix A Abbreviations

Chemical Compounds	
Abbreviation	**Chemical Name and/or Chemical Formula**
$Au_{1.5}$	AuNP with gold core of about 1.5 nm
$Au_{4.5}$	AuNP with gold core of about 4.5 nm
Mo-132a	$(NH_4)_{42}\left[Mo^{VI}_{72}Mo^{V}_{60}O_{372}(CH_3COO)_{30}(H_2O)_{72}\right]$ · ca. 300 H_2O · ca. 10 CH_3COONH_4
Mo-132b	$(NH_4)_{72-n}\left[\{(H_2O)_{81-n}+(NH_4)_n\}\subset\{(Mo^{VI})Mo^{VI}_5O_{21}(H_2O)_6\}_{12}\{Mo^{V}_2O_4(SO_4)\}_{30}\right]$ · ca. 200 H_2O
Mo-154	$(NH_4)_{28}\left[Mo_{154}(NO)_{14}O_{448}H_{14}(H_2O)_{70}\right]$ · 350 H_2O
TMA	N,N,N-trimethyl(11-mercaptoundecyl)ammonium chloride
	$C_{14}H_{32}ClNS$
TOAB	tetraoctylammonium bromide
	$C_{32}H_{68}BrN$

Other	
Abbreviation	**Term**
AuNP	Gold Nanoparticle
D_h	Hydrodynamic Diameter
DLS	Dynamic Light Scattering
IR	Infrared
IVCT	Inter-Valence Charge Transfer
NP	Nanoparticle
POM	Polyoxometalate
r	ratio of [POM]:[NP]
r_e	ratio of [POM]:[NP] at which electroneutrality in zeta potential results were observed
SAM	Self-Assembled Monolayer
SPR	Surface Plasmon Resonance
TEM	Transmission Electron Microscopy
TGA	Thermogravimentric Analysis
UV-Vis	Ultraviolet-Visible Spectroscopy

Appendix B Thermogravimetric Analysis

TGA experiments were performed by Jonathan Gooch. App. B Fig. 1 shows a representative analysis of the results when $Au_{1.5}$ was used as the sample. From this, it was determined that about 35% of the weight lost was from the TMA, and therefore about 65% of the total weight was the gold core. This mass percentage corresponds to approximately 101 gold atoms within the core, allowing for a range of 36 to 42 TMA ligands to be attached ($Au_{101}TMA_n$, where n = 36-42). These results were in agreement with previous reported studies.[46] Since each ligand has a +1 charge, the overall charge on the $Au_{1.5}$ lies between +36 to +42, although for simplicity was referred to as ≈42. TGA was also used to find the concentration of the $Au_{1.5}$ samples, since the small size of the gold core and the subsequent lack of a pronounced SPR band made the use of UV-Vis too difficult. A typical concentration was about 50 μM.

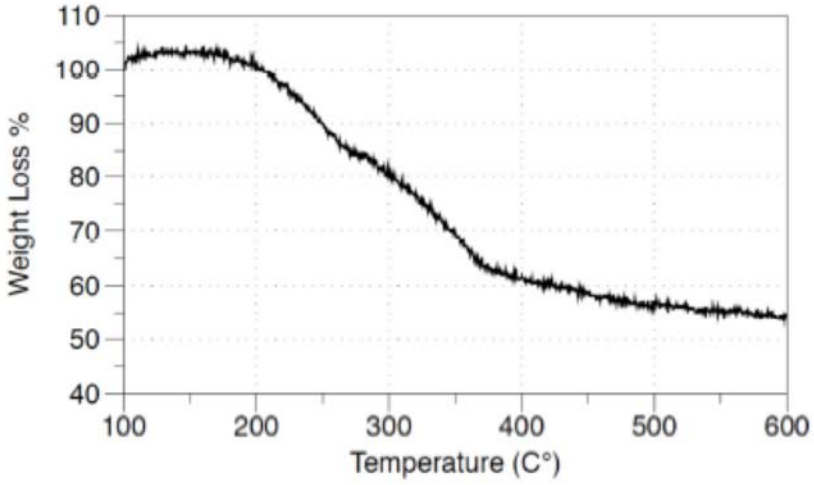

App. B Fig. 1: Representative TGA results for $Au_{1.5}$ to determine the mass of the gold core and the concentration of the $Au_{1.5}$ solution.